

Ion Beam Analysis of fusion plasma-facing materials and components: Facilities and Research Challenges

M. Mayer^{1*}, S. Möller², M. Rubel³, A. Widdowson⁴, S. Charisopoulos⁵, T. Ahlgren⁶, E. Alves⁷, G. Apostolopoulos⁸, N.P. Barradas⁵, S. Donnelly⁹, S. Fazinić¹⁰, K. Heinola⁵, O. Kakuee¹¹, H. Khodja¹², A. Kimura¹³, A. Lagoyannis¹⁴, M. Li¹⁵, S. Markelj¹⁶, M. Mudrinic¹⁷, P. Petersson³, I. Portnykh¹⁸, D. Primetzhofer¹⁹, P. Reichart²⁰, D. Ridikas⁵, T. Silva²¹, S. M. Gonzalez de Vicente⁵, and Y.Q. Wang²²

¹ Max-Planck-Institut für Plasmaphysik, 85748 Garching, Germany

² Institut für Klima- und Energieforschung, Forschungszentrum Jülich, 52425 Jülich, Germany

³ Fusion Plasma Physics, KTH Royal Institute of Technology, 100 44 Stockholm, Sweden

⁴ Culham Centre for Fusion Energy, Culham Science Centre, Abingdon, OX14 3DB, UK

⁵ International Atomic Energy Agency, Vienna International Centre, PO Box 100, 1400 Vienna, Austria

⁶ University of Helsinki, 00014 Helsinki, Finland

⁷ Instituto Superior Técnico, Universidade de Lisboa, 1049-001 Lisbon, Portugal

⁸ INRASTES, NCSR “Demokritos”, 15310 Aghia Paraskevi, Athens, Greece

⁹ University of Huddersfield, Ion Beam Centre, Queensgate, Huddersfield HD1 3DH, UK

¹⁰ Ruđer Bošković Institute, Bijenička 54, 10000 Zagreb, Croatia

¹¹ Nuclear Science and Technology Research Institute, P O Box 14395-836, Tehran, Iran

¹² LEEL, NIMBE, CEA, CNRS, Université Paris-Saclay, CEA Saclay, 91191 Gif sur Yvette Cedex, France

¹³ Kyoto University, Institute of Advanced Energy, Gokasho, Uji, 611-0011 Kyoto-Fu, Japan

¹⁴ Tandem Accelerator Laboratory, Institute of Nuclear and Particle Physics, NCSR “Demokritos”, 15310 Aghia Paraskevi, Athens, Greece

¹⁵ Argonne National Laboratory, 9700 Cass Avenue, Lemont, Illinois 60439, USA

¹⁶ Jožef Stefan Institute, Jamova cesta 39, 1000 Ljubljana, Slovenia

¹⁷ Vinca Institute of Nuclear Sciences, Belgrade, Serbia

¹⁸ Joint Stock Company Inst. of Nuclear Materials, Box 29, Zarechny, Sverdlovsk region, 624250 Russia

¹⁹ Department of Physics and Astronomy, Uppsala University, Box 516, 75120 Uppsala, Sweden

²⁰ Universität der Bundeswehr München, 85579 Neubiberg, Germany

²¹ Institute of Physics, University of São Paulo, CEP 05508-090 Cidade Universitária, São Paulo, Brasil

²² Los Alamos National Laboratory, Los Alamos, New Mexico 87545, USA

E-mail: matej.mayer@ipp.mpg.de

Received xxxxxx

Accepted for publication xxxxxx

Published xxxxxx

Abstract

Following the IAEA Technical Meeting on “Advanced Methodologies for the Analysis of Materials in Energy Applications Using Ion Beam Accelerators”, this paper reviews the current status of ion beam analysis techniques and some aspects of ion-induced radiation damage in materials for the field of materials relevant to fusion. Available facilities, apparatus development and future research options and challenges are presented and discussed. The analysis of beryllium and radioactivity-containing samples from future experiments in JET or ITER represents not only an analytical but also a technical challenge. A comprehensive list of

the facilities, their current status, and analytical capabilities comes alongside detailed descriptions of the labs. A discussion of future issues of sample handling and the current status of facilities at JET complete the technical section.

To prepare the international ion beam analysis community for these challenges, the IAEA technical meeting concludes the necessity for determining new nuclear reaction cross-sections and improving the inter-laboratory comparability by defining international standards and testing these via a round-robin test.

Keywords: Ion beam analysis, nuclear reaction, controlled fusion, first wall materials, beryllium, deuterium

List of Acronyms of Analysis Methods

| | | | |
|---------|--|------|---|
| AES | Auger Electron Spectroscopy | NRA | Nuclear Reaction Analysis |
| AFM | Atomic Force Microscopy | PALS | Positron Annihilation Lifetime Spectroscopy |
| EBS | (non-Rutherford) Elastic Backscattering Spectrometry | PAS | Positron Annihilation Spectroscopy |
| EDX | Energy Dispersive X-ray spectroscopy | PFC | Plasma-Facing Component |
| EPMA | Electron Probe Micro-Analysis | PIGE | Particle Induced Gamma Emission |
| ERDA | Elastic Recoil Detection Analysis | PIXE | Particle Induced X-ray Emission |
| HI-ERDA | Heavy Ion ERDA | PWI | Plasma-Wall Interactions |
| IBA | Ion Beam Analysis | RBS | Rutherford Backscattering Spectrometry |
| IBAD | Ion Beam Assisted (thin film) Deposition | SEM | Scanning Electron Microscopy |
| IBANDL | IBA Nuclear Data Library | SIMS | Secondary Ion Mass Spectrometry |
| IBIC | Ion Beam Induced Charge imaging | STIM | Scanning Transmission Ion Microscopy |
| IBIL | Ion Beam Induced Luminescence | STM | Scanning Tunnelling Microscopy |
| LEED | Low Energy Electron Diffraction | STEM | Scanning Transmission Electron Microscopy |
| LEID | Low Energy Ion Deposition | ToF | Time-of-Flight |
| LEIS | Low Energy Ion Scattering | TEM | Transmission Electron Microscopy |
| MEIS | Medium Energy Ion Scattering | UHV | Ultra High Vacuum |

1. Introduction

Plasma-wall interactions (PWI) in controlled fusion devices with magnetic confinement comprise all processes involved in the energy and mass exchange between the plasma and the surrounding materials and components [1-4]. Ions, electrons, charge-exchange neutrals, neutrons and electromagnetic radiation of a broad energy range cause severe modification of the physico-chemical and thermo-mechanical properties of wall materials and are responsible for erosion of plasma-facing components (PFCs). The main erosion mechanisms are: physical sputtering, chemical erosion, melting and melt layer splashing, evaporation, arcing, photo- and electron-induced desorption. Neutron irradiation changes properties not only of PFCs, but also of structural, functional (e.g. tritium breeders and diagnostics) and other materials affected by the neutron field.

As a consequence, there is need for detailed material analyses and for experimental simulation of radiation-induced damage. In both cases accelerator-based ion beam techniques play prominent roles either in ion beam analysis (IBA) or as tools for fast and efficient creation of radiation damage in solids for simulating certain effects connected with the impact of fast ions and neutrons. In these two inter-related fields of ion beam physics a number of issues have to be evaluated or re-assessed in order to further improve the reliability of data. These facts have motivated and laid grounds for the Technical Meeting on “Advanced

Methodologies for the Analysis of Materials in Energy Applications Using Ion Beam Accelerators” organized by the International Atomic Energy Agency (IAEA). The main goal was to review the current status and next steps in the following areas:

- Accelerator laboratories and their research potential for IBA of materials for fusion applications;
- IBA in fusion plasma-facing components and materials, including combinations of different ion beam methods;
- Fundamental aspects of employing ion beams for simulating radiation damage phenomena in materials for fusion energy production;
- Modelling tools and software development with emphasis on the analysis of materials employed in fusion applications;
- A cross-section database for IBA in fusion applications; data availability, exchange and further needs;
- A roadmap for future studies of fusion reactor materials using ion beam accelerators.

This paper provides a critical assessment of the status and further needs in IBA experiments and computer modelling. The aspect of ion induced radiation damage is related to IBA, but will not be covered here. First, main aspects of PWI are briefly introduced followed by a comprehensive overview of research capabilities in accelerator laboratories. Special requirements associated with studies of wall materials from fusion devices are discussed and strong emphasis is given to a holistic approach in handling of contaminated or activated

materials from fusion reactors and/or irradiation facilities. Research capabilities comprise also complex computer codes constituting fundamental tools for analysis and interpretation of IBA spectra. Their accuracy depends on the availability of evaluated data for stopping powers and cross-sections over a broad range of projectile energies and system geometries. Examples will be shown to illustrate difficult cases from the analytical point of view. The paper is concluded with a definition of specific tasks towards obtaining improved data sets for several projectile–target combinations and other requirements for successful IBA measurements for fusion research.

2. The role of ion beam analysis for plasma-wall interaction research

Plasma-facing materials and components are subjected to bombardment by charged and neutral particles escaping the plasma and by electromagnetic radiation related to electronic and nuclear processes. As a consequence, physical, chemical and thermo-mechanical properties of the wall materials are modified by physical sputtering, ion-assisted chemical erosion, implantation, melting, evaporation, arcing and – in the case of neutrons – by transmutation. At the same time the plasma is contaminated by species removed from the wall. Such impurity atoms are ionized when entering the plasma edge and are then transported along the magnetic field lines until they get re-deposited or pumped out. Re-deposition of all types of impurities present in the system together with hydrogen isotopes leads to the formation of co-deposited layers. These processes of erosion, re-deposition (with co-deposition) and potentially further re-erosion are responsible for material migration and mixing including the growth of fuel-rich mixed-material layers, i.e. co-deposits. Their detailed composition and structure cannot be foreseen a priori.

The main objective of PWI research is the determination of global changes of the plasma-facing wall in order to predict the lifetime of materials and components, the fuel inventory and the generation of dust by exfoliation of co-deposits, melting and splashing (in the case of metals) and brittle destruction (especially of carbon materials) under off-normal events and high local power loads.

The behavior and modification of materials under fusion-relevant conditions is studied in controlled fusion devices and in laboratory systems capable of simulating PWI processes by thorough material analyses before and after exposure to these extreme environments. The key point in analytical work is to achieve an as detailed as possible map of erosion and deposition zones, to determine material modifications, and to determine the influence of wall composition on the overall material migration. This includes the quantification of fuel retention in the bulk of wall materials and in co-deposited layers.

Figure 1 shows the interior of the vacuum vessel of the Joint European Torus (JET), located at the Culham Science Centre, United Kingdom. In figure 1(a) one perceives the great complexity of the plasma-facing wall: various types of limiters in the main chamber (details in the figure caption), protection of the central column (Inner Wall Cladding, IWC) and the divertor channel. Respective groups of PFCs are made of different materials (color-coded in figure 1b) to meet the operation criteria. Limiter tiles are made from bulk beryllium, while the recessed IWC tiles are made of cast Inconel. The majority of them is coated with evaporated beryllium, but in the upper part of the vessel Inconel is protected by a tungsten layer. Tungsten is used for divertor components either as coatings on carbon fibre composite (CFC) blocks in the outer and inner leg or bulk W lamellae for the outer divertor load bearing tiles. Detailed images of a few types of JET tiles are shown in figure 2. An important feature of all of those items is their size and – in some cases – significant weight. Therefore, the technical parameters of surface analysis stations must meet the criteria for handling such components; this point is discussed in Chapter 4.

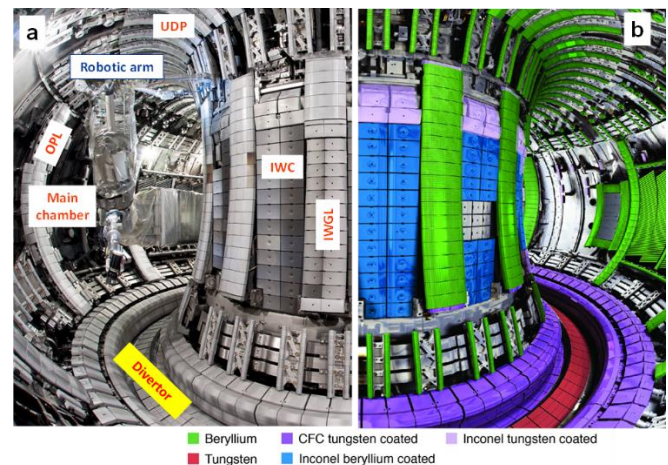


Figure 1. Toroidal view into the JET tokamak with the ITER-like wall (ILW): (a) structure of the plasma-facing wall; UDP: Upper dump plate; OPL: Outer poloidal limiter; IWC: Inner wall cladding; IWGL: Inner wall guard limiter; (b) colour-coded map of wall materials. The JET major radius is about 3 m.

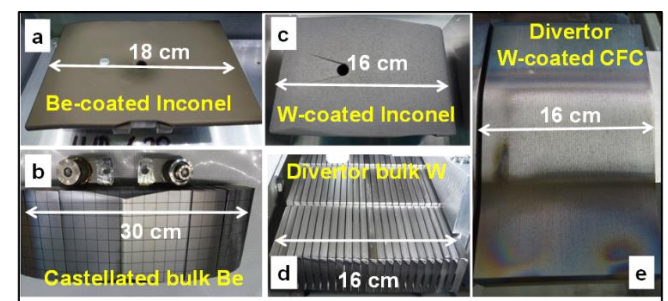


Figure 2. Examples of plasma-facing components from JET-ILW: (a) Beryllium coated Inconel tile from the inner wall cladding [81];

(b) segmented and castellated Be limiter tile [83]; (c) tungsten-coated CFC; (d) bulk tungsten divertor tile from the divertor base [81]; (e) tungsten-coated carbon-fibre composite (CFC) tiles of the inner and outer divertor [81].

Examined samples are selected wall components (limiters, divertor plates including marker tiles) and dedicated tools for erosion-deposition studies such as wall probes [5], retrieved from the device after short-term exposures (single discharges or series of experiments) or after entire experimental campaigns lasting up to 1×10^5 s. In detailed analyses of wall materials, the interest is in the determination of all species present in the reactor. These are hydrogen fuel isotopes (H, D, T), helium (He) originating either from the D-T fusion reaction or as fueling gas, constituents of main PFCs (C, Be, W), Fe, Cr, Ni, Mo, Nb as steel or Inconel components, elements used in plasma diagnostic systems (Mg, Al, Si) and for wall conditioning (He, Li, ^9Be , ^{10}B , ^{11}B , Si), common impurities (C, O), gases seeded for plasma edge cooling (N, Ne, Ar, Kr, Xe) and tracers for material migration introduced deliberately to the studied system in minute quantities (^6Li , ^7Li , ^{10}Be , ^{13}C , ^{15}N , ^{18}O , ^{19}F , ^{21}Ne , ^{22}Ne , Hf, Re etc.).

Over the years more than fifty different material research methods have been used for the analysis of PFCs and of probes exposed to plasmas in fusion devices and simulators of PWI. Accelerator-based IBA methods are crucial in this field due to their sensitivity, depth-profiling ability, and quantification without need for reference samples. The IBA family comprises nine major members: nuclear reaction analysis (NRA), elastic recoil detection analysis (ERDA) including high-energy heavy ion variants (HI-ERDA with e.g. incident C^{n+} , Si^{n+} , $^{127}\text{I}^{n+}$, Au^{n+}), Rutherford backscattering spectrometry (RBS), non-Rutherford elastic backscattering spectrometry (EBS), medium energy ion scattering (MEIS), particle-induced X-ray and gamma-ray emission (PIXE and PIGE, respectively) and accelerator mass spectrometry (AMS). However, taking into account the large variety of used beam energies, projectiles, and beam-target-detector geometries a huge number of widely used and

very specifically tailored techniques is available. Their role has been very clearly proven in hundreds of analytical works from many laboratories involved in material studies from nearly all fusion devices around the world.

3. Research capabilities: ion beam laboratories in studies of reactor materials

A prerequisite for comprehensive material studies are well equipped laboratories, experienced staff, and international cooperations. The research capabilities of several accelerator laboratories working in the field of fusion materials are presented in this section. Main characteristics of the facilities are listed in Table 1; detailed descriptions are presented in sections A.1 – A.13 and schematic drawings of the facilities are shown in Figures A1 – A13 (only online version). It should be stressed that this listing comprises only facilities represented at the IAEA Technical Meeting and is not representing any quality rating in any order.

In addition to the facilities listed in Table 1 and described in sections A.1 to A.13 the following facilities are active in IBA for fusion research:

- Sandia National Laboratories, Albuquerque, New Mexico, USA [69].
- Massachusetts Institute of Technology, Plasma Science and Fusion Center, Cambridge, Massachusetts, USA [70-72].
- Fudan University, Institute of Modern Physics, Shanghai, China [73].

Facilities for ion induced radiation damage are related to IBA facilities, but have their own specifics and cannot be covered here completely. The following facilities are described in sections A.14 and A.15:

- University of Huddersfield, MIAMI Facility, Huddersfield, United Kingdom [74], see section A.14 and Fig. A14.
- Argonne National Laboratory, IVEM-Tandem Facility, Illinois, USA [75-77], see section A.15 and Fig. A15.

Table 1. IBA facilities active in the analysis of samples from fusion devices and their analytical possibilities.

| Laboratory, Country | Accelerator | Available beams | Beamline | Methods available |
|---|------------------|--|----------|---|
| Uppsala University, Tandem Laboratory, Uppsala, Sweden [6-12] | 5 MV Tandem | H, D, ^3He , ^4He , Li, and heavier ions | 1 | NRA (gamma & particle), RBS |
| | | | 2 | NRA, RBS, PIXE, μ -beam |
| | | | 3 | AMS tracer experiments for Be |
| | | | 4 | chamber 1: RBS, NRA (gamma & particle), PIXE, TOF-ERDA; chamber 2: RBS, NRA (gamma & particle), PIXE, TOF-ERDA, large samples; chamber 3: RBS, NRA for cross section measurements |
| | | | 5 | irradiation: 2 MeV to several ten MeV |
| | | | 6 | in-situ growth and modification, RBS, NRA (gamma & particle), PIXE |
| | 350 kV Implanter | H, D, ^3He , ^4He , Li, and heavier ions including molecular ion beams | 1 | implantation >2 keV, broad range of elements, RT - 800K |
| | ToF-LEIS | | 2 | ToF-MEIS with 2 PSD-detectors |
| | | | 3 | Low-energy HR-RBS & NRA, irradiation, cryostatic detector |
| | | H, D, ^3He , ^4He , Ne, Ar including molecular ion beams | 1 | ToF-LEIS with charge separation, AES, LEED, in-situ growth and modification |
| INPP, NCSR | 5.5 MV Tandem | H, D and heavier ions | 1 | Nuclear Astrophysics, Hydrogen Profiling |

| | | | | | |
|--|--|--|---|--|---|
| "Demokritos", Tandem Accelerator Laboratory, Athens, Greece [13-15] | | | 2 | μ-beam | |
| | | | 3 | chamber 1: RBS, NRA, PIGE chamber 2: PIXE | |
| | | | 4 | setup 1: gamma angular distribution turntable setup 2: goniometer table for cross section measurements | |
| | | | 5 | Atomic Physics | |
| | | | 6 | setup 1: fast neutron production setup 2 : Ion irradiation with in-situ electrical Resistivity measurement | |
| | | | Instituto Superior Técnico, Universidade de Lisboa, Ion Beam Laboratory, Lisbon, Portugal [16-20] | 3 MV Tandem and 2.5 MV van de Graaff | H, ³ He, ⁴ He and heavier ions |
| 2 | NRA, RBS, PIXE, IL, STIM, μ-beam (with external beam) | | | | |
| 3 | μ-AMS optimised for heavy elements | | | | |
| 210 kV Implanter | nearly all periodic table | 1 | | implantation >2 keV, broad range of elements from 77 to 1273 k | |
| | | 3 | | In-situ implantation and IBA from 77K to RT | |
| CEA/Saclay, Laboratory for Light Element Studies (LEEL), France [21,22] | 3.5 MeV single ended van de Graaff | H, D, ³ He, ⁴ He | 1 | μbeam for PIXE, RBS, NRA, PIGE, ERDA, ERCS + in situ low Energy light ion implantation | |
| | | | 2 | μ-beam for RBS, NRA, ERDA, Beamline dedicated to highly radioactive samples (analysis chamber in a concrete cell; β/γ emitters accepted, pure α or neutron sources not allowed) | |
| Vinca Institute of Nuclear Sciences, User Facility for Irradiation and Analysis of Materials with Ion Beams, Belgrad, Serbia [23,156] | CAPRICE: ECR ion source. Heavy ion beams: 10-20 keV/amu; light ions: 15-30 keV | H, D, ³ He, ⁴ He, Li, and heavier ions | | Ion Beam Assisted Deposition (IBAD), Ion Bombardment irradiation of polycrystalline targets in the temperature range from 252 to +353 K, and implantation of monocrystalline targets in the temperature range from 173 to 1273 K | |
| | Cyclotron, energies 1 to 3 MeV | H | | The characteristics of the proton beam: energy precision – below 1 keV; energy spread – below 0.1 %; current 10 to 100 nA. RBS, PIXE, NRA, PIPS Detector (p, α), Si X-Ray detector and cryostat | |
| Forschungszentrum Jülich, Tandetron Laboratory, Jülich, Germany [24-27] | 1.7 MV Tandem | H, D, ³ He, ⁴ He | 1 | μ-Beam, NRA, RBS, PIXE, PIGE, Irradiation: 0.5-3.5 MeV @350 nA, temperature monitoring, electrical contacts, 4-point resistivity measurement, non-flaking Be possible | |
| | | | 2 | free | |
| | | 3 | TDS 77-1200 K, XPS, NRA, RBS, Plasma loading/implantation, AES, Be compatible | | |
| 15-30 MeV Cyclotrons | H, D, ⁴ He | 1 | Irradiation: 10 to 100 μA/cm ² , temperature monitoring, remote handling of extremely active samples | | |
| | | 45-200 MeV Cyclotron | H, D | 1 | Irradiation: 1μA/cm ² , temperature monitoring, active samples |
| | | Maier-Leibnitz-Laboratory (MLL), Garching, Universität der Bundeswehr München, Neubiberg, Germany [28-30] | 14 MV Tandem | H, D, ³ He, ⁴ He, Li, and heavier ions | 1 |
| 2 | Q3D Magnetspectrograph: heavy ion ERDA, high resolution ERDA | | | | |
| 3 | AMS: High-Energy AMS system with gas filled magnet system | | | | |
| Rudjer Boskovic Institute, Tandem Accelerator Facility, Zagreb, Croatia [31-36] | 6 MV Tandem and 1 MV Tandetron | H, ³ He, ⁴ He, Li, and heavier ions | 1 | PIXE, PIGE, RBS (available with 1 MV Tandetron only) | |
| | | | 2 | in air PIXE (available with 1 MV Tandetron only) | |
| | | | 3 | dual beam: focused ion beams (microprobe) from 1 MV Tandetron, broad beam from 6 MV Tandem; ion beams available simultaneously from both accelerators | |
| | | | 4 | dual beam irradiation chamber; ion beams available simultaneously from both accelerators | |
| | | | 5 | Capillary MeV TOF-SIMS, ToF-ERDA | |
| | | | 6 | ion beams available from both accelerators | |
| | | | 7 | RBS/RBSc, PIXE/PIXEc (channeling), NRA, ion beams available from one or the other accelerator | |
| | | | 8 | cross sections measurements, ion beams available from one or the other accelerator | |
| microprobe - RBS, PIXE, NRA, IBIC, HR-PIXE (with focused ion beams), ion beams available from one or the other accelerator | Max-Planck-Institute for Plasma Physics, Tandem Laboratory, Garching, Germany [37-42] | H, D, ³ He, ⁴ He, Li, and heavier ions | 1 | Chamber 1: RBS, NRA, ERDA (with He, Li, ¹² C, ¹⁶ O beams); Chamber 2: RBS, NRA, PIGE, large samples ≤300×200×100 mm ³ | |
| | | | 2 | Chamber 1: Irradiation: 200 keV to several 10 MeV; Chamber 2: RBS, NRA, ToF-RBS | |
| | | | 3 | RBS, NRA for sample sizes up to 100×20×20 mm ³ , Glove box for Be contaminated samples, T up to 1 GBq | |
| | | | 4 | RBS, NRA, ERDA, in-situ irradiation and implantation with 2 ion sources | |
| Nuclear Science and | 3 MV Van de | H, D, ⁴ He, N including | 1 | NRA (gamma & particles), RBS | |

| | | | | |
|--|---|--|--|--|
| <i>Technology Research Institute, Van de Graaff laboratory, Teheran, Iran</i> [43-48] | Graaff | molecular ion beams | 2 | RBS-channeling, RBS |
| | | | 3 | RBS, PIXE, NRA (particles) |
| | | | 4 | Irradiation: 300 keV - 3 MeV / External PIXE / K-edge contrast Imaging / IL spectroscopy & Microscopy |
| | | | 5 | RBS, NRA (particles) |
| | | | 6 | NRA, RBS, PIXE, IBIL, μ -beam |
| | | | <i>Jožef Stefan Institute, Microanalytical Centre, Ljubljana, Slovenia</i> [49-55] | 2 MV Tandem |
| 2 | μ -beam - PIXE, RBS, NRA, MeV-SIMS | | | |
| 3 | in-situ D exposure/ thermal treatment; RBS, NRA, ERDA | | | |
| 4 | High resolution XRS | | | |
| <i>Los Alamos National Laboratory, Ion Beam Materials Laboratory, New Mexico, USA</i> [56-63,157] | 3 MV Pelletron Tandem Accelerator | H, D, ^3He , ^4He and heavier ions | 1 | Standard IBA techniques (RBS, NRA, ERD, PIXE, channeling). |
| | | | 2 | Self-ion high temperature irradiation/implantation under LN2 to 1000 C, ion irradiation and corrosion experiment |
| | | | 3 | He implantation to simulate material compatibility in actinides |
| 4 | | | Alpha radiolysis research in solids, liquids, and gases | |
| 5 | | | Dual-beam chamber between Tandem Accelerator and Varian Impanter (LN2 to 1523 K) | |
| | 200 kV Varian Implanter | Mainly gas ion species | 1 | implantation/irradiation: 5 keV to 200 keV ions under LN2 to 1250 C |
| | 200 kV Danfysik Implanter | Virtually any ions, including metals | 1 | implantation/irradiation: 20 keV to 800 keV ions under LN2 to 500 C |
| <i>University of Helsinki, Accelerator Laboratory, Helsinki, Finland</i> [64-68] | 5 MV Tandem | H, D, Li, and heavier ions | 1 | NRA (gamma & particle), RBS |
| | | | 2 | NRA, RBS, PIXE |
| | | | 3 | AMS |
| | | | 4 | chamber 1: RBS, NRA, PIXE, Tof-ERD; chamber 2: RBS, Stopper foil-ERDA; chamber 3: PAS |
| | | | 5 | irradiation: 1 MeV - several ten MeV |
| | | 500 kV Implanter | H, D, ^3He , ^4He , Li, and heavier ions including molecular ion beams | 1 |
| | | | 2 | ^3He NRA |
| | | | 3 | Low-energy RBS & NRA, irradiation |

4. Specific issues in studies of fusion reactor materials

There are a number of requirements in handling, transportation and analyses of fusion reactor materials. In addition, there are also serious restrictions in particular when working with materials originating from the JET tokamak with beryllium wall components and the presence of tritium related both to the operation with deuterium – tritium (D-T) fuel and produced in D-D nuclear reactions. Manual access is very limited. The removal, repair and replacement of selected tiles of PFCs and of erosion-deposition monitors is performed only during major shut-downs using a remotely handled (RH) robotic arm. All items retrieved from JET are transferred to the Beryllium Handling Facility (BeHF) at Culham Science Centre. All operations aiming at the dismantling, installation of items from the divertor modules or so-called wall brackets are carried-out in glove boxes by personnel wearing pressurized suits.

4.1 Characteristic of wall components

Obviously the entire surface area of a fusion device cannot be analysed due to time and cost constraints. For tokamaks with toroidal symmetry it is necessary to analyse at least one poloidal cross-section of the machine in order to be able to extrapolate to the whole machine. For tokamaks without toroidal symmetry (for example due to individual poloidal limiters) or stellarators (which do not have toroidal symmetry) multiple poloidal cross-sections may become necessary. Plasma-facing surfaces are typically made of

separate wall tiles which can be dismantled and analysed individually. Although even single tiles may be large and heavy (see below), they are still much smaller than a whole component, such as a whole divertor section. Water-cooled components can be problematic because these cannot be removed without separation from the water feeds [78]. Decommissioned machines provide a vast amount of components for analysis [79], but the interpretation of data after very long exposures may be challenging.

In most cases material and manufacture of PFC tiles is expensive, therefore, these are often unique components without spares for replacement. Significant costs are also involved in the retrieval of tiles using remote handling systems. Therefore, the expenditure related to procurement and RH operation has to be taken into account in the planning of tile retrieval. Tiles without spares, if analysed ex-situ, must be returned to JET for re-assembly during the same shut-down. For obvious reasons, cutting or any shape-changing sampling from such tiles is strictly excluded. This implies that dedicated surface analysis stations need to be equipped with chambers accommodating large and heavy items. For instance, the W-coated CFC divertor tile shown in figure 2(e) has dimensions of $5 \times 16 \times 25 \text{ cm}^3$ and a weight above 2 kg. Hemispherical bulk tungsten test limiter tiles from the TEXTOR tokamak has a weight even above 8 kg. Analyses of such components requires chambers with large loading ports and manipulators with long travel distance and potentially three-axis rotation.

A schematic drawing of a chamber housing several types of detectors used for IBA of large tiles is shown in figure

3(a), while figure 3(b) shows a precision manipulator (50 μm accuracy) for handling heavy test limiters such as bulk tungsten and B₄C-coated copper presented in Fig. 3(c,d), respectively [80].

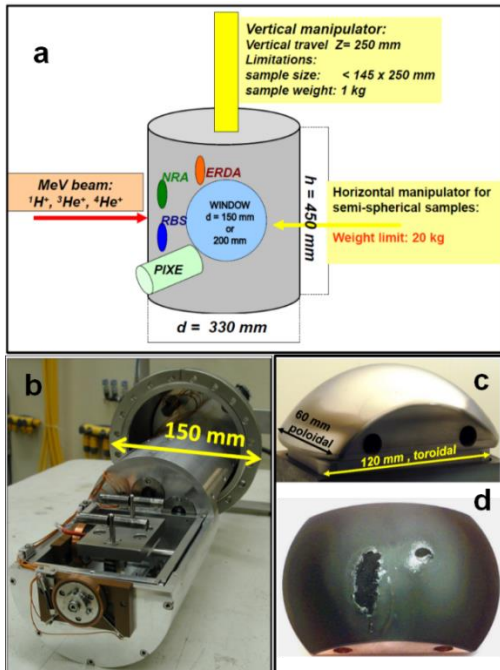


Figure 3. (a) Schematic drawing of a surface analysis station with the capability for handling large and heavy PFC tiles; (b) precision manipulator holding heavy test limiters [152] shown in (c) [155] and (d) [80]. The coating on the limiter in (d) has been partly molten.

Tiles which have spares can be sectioned to provide samples for different types of surface and bulk analyses. Cutting into small pieces reduces also the activity of samples to be handled in laboratories involved in studies of contaminated materials from JET [81]. This also allows very detailed high-resolution mapping by micro-beams, depth profiling, preparations of samples for transmission electron microprobes and, as result, it leads to conclusions on the overall material erosion-deposition pattern in a fusion device. W-coated CFC tiles are “cored” in the form of cylinders (8 or 18 mm in diameter). CFC coring procedures were developed in connection with the analyses of tiles after a full D-T campaign in JET, 1997-1998, when the activity of tritium accumulated in single tiles exceeded 100 GBq [82]. Figure 4 shows a schematic drawing of a tile with two adjacent rows of cored samples: one set for the tritium determination by full combustion followed by scintigraphy of tritiated water and the other one for D, Be, C measurements with ³He-based NRA and metal impurities with RBS. The operation of JET-ILW called for the development of methodologies for beryllium, tungsten and Inconel cutting in order to provide samples for microscopy, IBA, thermal desorption etc. The metals are sawn under strict temperature control (infrared

cameras, max. 60°C) during that procedure to avoid desorption of hydrogen isotopes. Figure 5 provides details on the structure of the segmented castellated beryllium limiter tiles and their sectioning into single blocks of castellations in order to facilitate further detailed studies [83].

4.2 Requirements for handling fusion materials

The analysis of materials from fusion devices will necessarily require laboratories to handle some level of tritium, beryllium and/or activated samples. The presence of these hazards, particularly in combination, is problematic for many laboratories. However, experience of handling such samples has been gained from the plasma facing materials analysis programme at JET where beryllium has been used since 1990 and the first deuterium-tritium plasmas were performed in 1997 [84]. In 2010 the main chamber PFCs were exchanged for Be and the divertor PFCs for W to allow operations with an ITER-like wall configuration. This change increased the amount of Be to be handled for analysis. Due to the presence of beryllium, tritium and activated nuclides it is not acceptable to remove samples for analysis from JET on an *ad hoc* basis, given that a significant amount of planning for the remote installation and removal of samples is needed. Specialised facilities are also required to recover the samples to make them available for analysis. At JET samples are handled in the Beryllium Handling Facility dedicated for working with beryllium and tritium contaminated components, as shown in figure 6.

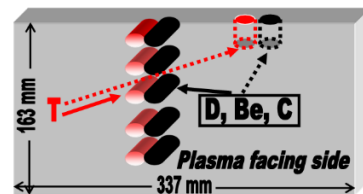


Figure 4. Schematic drawing of sectioning by coring large CFC-based divertor tiles from JET [152].

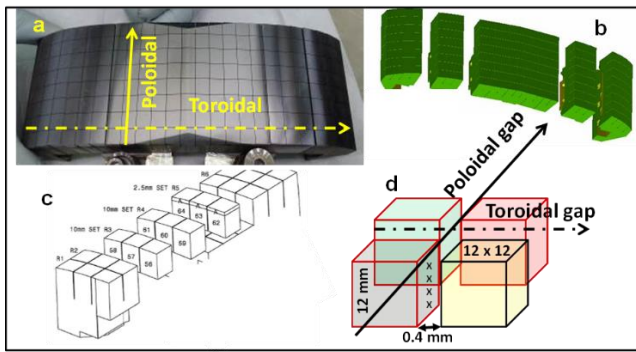


Figure 5. Details of the structure and sectioning of castellated beryllium limiters from JET: (a) appearance of the outer poloidal limiter and (b) the segmented tile structure; (c) sectioning and marking scheme of single blocks of castellations to enable micro-beam analyses in the gaps (d). The analysis line is marked with X.

Therefore, to gain the most information from the analysis programme the complete cycle must be considered at the outset:

- sample planning – type of sample, exposure location, analysis aims;
- sample handling post exposure – size of samples, cutting, transport, contamination evaluation;
- ion beam facility capabilities – contamination containment, neutron shielding, radiation monitoring, beryllium monitoring.

4.3 Sample planning

The main aim of the analysis programme is to provide long term fuel retention and material erosion, migration and deposition assessment for fusion devices. The results provide insight into the physical processes of plasma wall interaction and results for benchmarking modelling codes. In order to facilitate the programme the analysis aims need to be well understood, this in turn guides the sample type and location in the vessel. The basic strategy is to analyse a set of representative plasma facing components. The analysis data from PFCs may be enhanced by using marker coatings deposited onto surfaces or by the injection of isotopically labelled gases at the end of the operating period as discussed in section 2. In the case of marker coatings the thickness of the coating must be analysed before and after exposure using

backscattering techniques in order to determine erosion and deposition. Some lessons learned from JET highlight the need for choosing a material for the interlayer that is dissimilar from other species found in the local environment and also ensuring good adhesion of the coatings and matched thermal coefficient of expansion to decrease the risk of delamination from the PFC surface. The detection of the isotopes on PFC surfaces using IBA can be used to map migration from the injection point.

Specifically designed diagnostics aiming at providing time resolved erosion/deposition patterns [84], gross deposition and sticking coefficients [85] of deposited material have been deployed in fusion devices. Such diagnostics are typically installed in locations remote from the plasma, thus providing data on long range material migration to remote regions [86].

4.4 Sample handling and facility capabilities

To maintain a successful analysis programme of contaminated samples the participating laboratories need to have compatible infrastructure for sample handling. This is not only in respect of analysis but there may also be a need for resources in accounting and monitoring of radioactive materials and/or beryllium in order to transport and store samples.

In the case of analysis, glove boxes or containment isolators need to be attached to the analysis chamber to allow for the manipulation of contaminated samples. This type of containment is available at IST, Portugal, figure 7 and IPP Garching, Germany, figure 8. In the case of deuterium ion beam based Be samples analysis, additional shielding is required such that available at Demokritos, Greece, section A.2, and University of Helsinki, Finland, section A.13.

Within the JET analysis programme the only laboratory capable of routinely handling whole PFCs as shown in figure 2, is at IST, Portugal, described in section A.3. The ability to handling these samples is due to the infrastructure at the site for accepting samples containing tritium and beryllium, the installation of a containment isolator on the chamber, see figure 7, the size of the analysis chamber and ability to manipulate the component in the beam by 150 mm in height. An advantage of handling whole tiles is that expensive components can be analysed non-destructively and returned to the machine. Analysis of whole components also avoids complicated reconstruction of data plotting arising from many smaller samples.



Figure 6. Operatives working in the Beryllium Handling Facility [81], a facility for supporting JET operation and maintenance. (a) and (b) Operative are wearing air inflated hoods equipped with a filter, disposable coveralls, rubber boots with overshoes and several pairs of gloves including a sacrificial top layer which is changed periodically. Work on JET components is carried out in ventilated slit boxes to minimise the spread of contamination and exposure to operatives. (c) Where it is not possible to work within a slit box, operatives wear a full containment suit with dedicated pressurised air supply.

However, to take advantage of the range of techniques offered by IBA it is necessary to provide smaller samples for analysis. The reduction in size not only allows the samples to be mounted at the analysis station but also reduces potential hazards associated with handling the sample. In the case of JET PFCs the radioactive inventory and beryllium levels of smaller samples are low enough to be accepted at participating laboratories and are relatively straightforward to transport in accordance with regulations. Depending on the size and number of samples it may still be necessary at some laboratories to provide containment at the analysis station, for example, as shown for IPP Garching in [figure 8](#). Smaller samples can be in the form of specifically designed, easily removable tokens from larger components or samples cut from larger components. Current cutting capabilities are available for JET tiles consisting of tungsten coated carbon fibre composite, bulk beryllium and bulk tungsten. In all cases the methods are dry cutting techniques and temperature controlled to minimise the dissolution or desorption of fuel from the component [87].

With this type of infrastructure, capability for sample cutting and resources for controlling transport and on site monitoring, it has been possible to facilitate the analysis of beryllium and tritium contaminated samples from JET. However, based on the estimations of tritium inventories and activation in PFCs following JET deuterium-tritium operations, of neutron irradiated samples and of future fusion devices such as ITER will make sample transport and preparation significantly more demanding in terms of radiation safety. In these cases sampling handling and cutting facilities involving hot cells will be required.

4.5 Analysis techniques and data analysis of JET samples

Whilst in many respects samples share characteristics, in reality each sample is unique as it has been exposed to a wide variety of plasma operating conditions at its individual location and exposure time. Long and varied exposure to plasma means that the samples are highly inhomogeneous which places challenges on the IBA techniques employed for

analysis. For example, the surface of PFCs may be fully covered with rough or smooth deposit, may be partially eroded or partially deposited or may have been melted. Deposits on the samples may be tens of microns thick and have inhomogeneous thickness, composition and density. The main techniques used to characterise these types of samples from JET are NRA and PIXE using the facilities at IST, Portugal ([section A.3](#)), and IPP Garching, Germany ([section A.9](#)). From this analysis depth profiles of deposits, fuel retention and erosion of marker coatings are studied. However, data analysis has to take into account the inhomogeneity of the sample, see [section 6.1](#). HIERDA at Uppsala, Sweden ([section A.1](#)) and University of Helsinki, Finland ([section A.13](#)) is used mainly for smooth samples, such as on the dedicated passive diagnostic surfaces. Microbeam techniques at RBI, Croatia ([section A.8](#)) are useful for mapping inhomogeneities in deposits or small dust samples. Deuterium beam enables carbon and oxygen impurities to be evaluated in beryllium deposits. This analysis is carried out at Demokritos, Greece ([section A.2](#)).

With these targeted IBA techniques and data analysis the results provide insight into fuel retention and material migration. However, in order to achieve these results, data analysis must take into account the inhomogeneity of the samples, as discussed in [sections 5 and 6](#). This experience gained with JET is the basis for all other IBA activities for future fusion experiments such as W7-X or ITER.

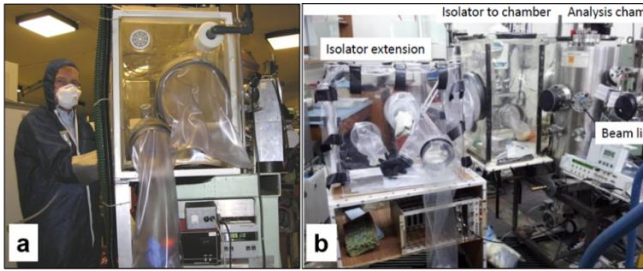


Figure 7. (a) Operative working at isolator loading samples into analysis chamber. (b) Analysis station at IST Lisbon showing analysis chamber with main isolator and extension for handling whole JET tiles contaminated with tritium and beryllium.

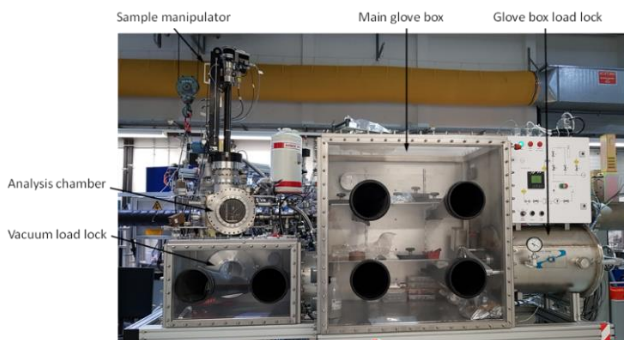


Figure 8. Glove box system at IPP Garching consisting of a glove box load lock, a main glove box for sample storage and handling, a secondary glove box for transferring samples to vacuum, a vacuum load lock between vacuum system and glove box, a sample manipulator for sample transfer between the vacuum load lock and the analysis chamber and for sample manipulation, and the analysis chamber with various detectors.

4.6 Effects of air exposure

The vast majority of IBA measurements of samples from fusion devices are performed ex-situ, i.e. the samples were stored for a typical time of several days to several months in air. The main reason are the huge technical difficulties associated with an IBA system in a reactor-class device keeping in mind the radiation field (n, X and gamma), the permanent magnetic field, temperature excursions of plasma-facing components, and difficulties to maintain/repair equipment. Moreover, in-situ IBA gives only information from a limited number of areas inside the vessel that are accessible by the incident ion beam and have free sight to the detector(s). An in-situ IBA system was used at Alcator-C Mod using an incident deuterium beam and detecting gamma radiation (PIGE) [71,72].

In-vacuo analysis has been employed at JET by the Fast Transfer System allowing the transfer of samples from the JET vessel to accelerator laboratories under vacuum. However, the high technical complexity made the use of this system very difficult and highly impractical. As a result, it was used only on very rare occasions [88]. A vacuum “suitcase” allowing the transfer of a sample in vacuum from

the ASDEX Upgrade midplane manipulator to the SAK analysis station was foreseen at ASDEX Upgrade [89], but, to our knowledge, was never used.

However, in-situ IBA is used in a number of laboratory experiments for simulating specific aspects of PSI processes (e.g. [90]).

Many results are not affected by exposure to ambient atmosphere at all: For example the amounts of eroded or deposited solid materials (such as beryllium, carbon or tungsten) are not altered by air exposure. These data provide important information about erosion/deposition processes, material transport and component lifetime. The major risks of material exposure to ambient atmosphere are related to: (i) isotope exchange of deuterium or tritium by hydrogen from water vapour present in humid air and (ii) oxygen reaction with surfaces.

(i) The instant release or isotope exchange of hydrogen isotopes under contact of PFCs with ambient atmosphere cannot be excluded. For practical reasons the shortest time between the exposure and analysis are several hours. The retention data obtained after that time and a few days later were identical [91]. There were also exercises of measuring the same sample after a few years of storage, and a decrease by 25% was observed after 5 years [91]. The deuterium content of a deuterated amorphous hydrocarbon layer was stable within the measurement uncertainties during 8 years of storage in ambient atmosphere [92], while the D content of a sample from ASDEX Upgrade decreased by a factor of about 2 within roughly 1 year [92]. A radiation-damaged W sample was implanted by 8 eV D ions at 370 K, the D-content decreased by less than 15% during a storage time of 1.5 years [93]. If a massive release occurs, it probably happens immediately after air ingress. For that reason IBA data are compared with the global gas balance which indicated the retention to be 30-50 % larger than that obtained with ex-situ IBA [94]. Depending on material structure the release of hydrogen isotopes from samples from fusion devices can be an issue, but according to current knowledge this release is assumed to be relatively slow. Laboratory samples are usually stable over long periods of time.

(ii) Oxidation of surfaces and/or uptake of water molecules from humid air is an issue. Therefore the interpretation of the oxygen and protium signals has to be very carefully. Comparison to reference samples and laboratory experiments can help to determine the effect of oxidation.

5. Simulation Programmes

Except for very simple cases the calculation of damage- and implantation profiles or the quantitative evaluation of IBA spectra requires the use of simulation software. Many codes dedicated for calculating energetic ion-solid interactions, IBA spectrum simulation and quantitative IBA

data analysis have been developed over the last decades. It is beyond the scope of this paper to review all of them, a short overview of codes relevant for fusion research is given below.

Molecular Dynamics (MD): MD calculates the time evolution of trajectories of a set of interacting atoms by numerical integration of Newton's equation of motion [95]. The forces between the particles and their potential energies are determined using interatomic potentials, the time steps are typically of the order of a few fs each. MD simulations are very close to physical reality but require long computing times and are usually limited to short timescales below 1 μ s. In materials science MD is used for calculating various aspects of radiation damage by energetic ions [96], ion ranges in materials [97], and ion channelling [98]. Multiple molecular dynamics software packages with similar core functionality are available.

Monte Carlo (MC) with binary collision approximation (BCA): In BCA the trajectory of an energetic ion in a material is approximated by a sequence of independent binary collisions with sample atoms; the ion trajectory between these collisions is assumed to be straight and experiencing electronic energy loss but no further collisions with nuclei [99]. BCA simulations are much faster than MD simulations, but are limited to higher energies due to the neglect of many-body interactions taken into account by MD. The target structure is often assumed to be amorphous. BCA simulations are a common tool for calculating reflection, sputtering, radiation damage and ion ranges in materials. MC with BCA is generally too slow for analysing IBA energy spectra on a regular basis but has been used for calculating MEIS [100] or RBS spectra in special cases [101]. The most popular BCA code is SRIM [102], but different codes (for example SDTrim.SP [103]) are available and may offer improved accuracy [104].

MC with BCA and weight function: This family of codes is optimised for fast calculation of RBS and ERDA energy spectra including accurate simulation of plural (large angle) and multiple (small angle) scattering effects. In contrast to classical MC with BCA these codes do not calculate individual particles, but ensembles of particles using MC summing up probabilities instead of single particles for obtaining the energy spectra. Only particles with sufficiently high probability to reach the detector are followed, and a much larger detector than the real one ('virtual detector') can be used. These codes are typically several orders of magnitude faster than MC with BCA codes and fast enough for calculating RBS and ERDA spectra on a regular basis, available codes are MCERD [105,106] and CORTEO [107].

Analytical codes: This family of codes approximates the trajectories of incident and exit particles by straight lines connected by a single scattering or reaction event, incident

and exit particles experience electronic and nuclear energy loss and energy loss straggling on their trajectories. Modern codes approximate multiple scattering effects as energy spread [108]; plural scattering is approximated in the dual scattering approximation [101]. Many different codes exist in this family and have been reviewed in [109]. Codes typically include data bases for different stopping and straggling models and sometimes incorporate data bases for non-Rutherford scattering, nuclear reaction and PIGE cross-sections. Sample effects like porosity or various surface roughnesses and detector effects like geometrical straggling, dead time or pulse pile-up can be included in simulations. These codes are generally very fast and are regularly used for evaluating RBS, EBS, ERDA, NRA, MEIS, and PIGE spectra. Popular codes are SIMNRA [110,111], NDF with graphical user interface WinDF [112], and RUMP [113]. An intercomparison of analytical codes was presented in [114,115] and showed very good agreement.

Self-consistent analysis of multiple measurements: Complex samples with multiple elements often require the analysis of multiple measurements using different methods and/or different energies or geometries. This analysis should be self-consistent, i.e. a unique sample structure should be used for all simulations. NDF/WinDF [112] and MultiSIMNRA [116] provide self-consistent analysis of multiple IBA measurements, NRADC [117] has been developed for depth-profiling of deuterium using measurements at different energies. SIMNRA [110,111] offers full access to its functionality through COM/OLE interfaces, thus allowing automated data processing.

Codes for 2- and 3-dimensional samples: Samples with artificial surface structures (e.g. periodic gratings [118]), extreme surface roughnesses (e.g. tungsten fuzz [119]), or heterogeneous materials [120] require specialized codes. SDTrimSP-2D [121] is a MC code with BCA allowing calculating the evolution of 2-dimensional targets by implantation and sputtering [113]. CORTEO [107] allows calculating IBA spectra from arbitrary 2-dimensional or 3-dimensional material distributions [122]; STRUCTNRA [123] calculates IBA spectra from arbitrary 2-dimensional distributions. A recent inter-comparison of different codes showed very good agreement among the codes and with experimental data [124].

Samples from fusion experiments are often highly challenging for all analysis methods including ion beam analysis: In many cases low-Z and high-Z elements are present in the samples, requiring multiple measurements with different techniques (for example RBS for high-Z elements, NRA for low-Z elements, and PIXE/PIGE for trace elements) and self-consistent data analysis. The required depth of analysis can exceed several 10 μ m: RBS measurements then need high-energetic protons with energies above 3 MeV. The scattering cross-sections are non-

Rutherford for all lower-Z elements at these energies, while the presence of high-Z elements can result in distinct multiple and plural scattering effects. Redeposited and eroded layers can be laterally inhomogeneous, both with respect to layer thickness and composition. Sample surfaces are often technically rough, in some cases carbon-fibre composite (CFC) surfaces with very high roughnesses are to be analysed. The number of measured spectra can exceed several thousand, setting limits to the possibilities of manual data analysis and requiring automatic procedures with as little manual intervention as possible.

These challenges raised by the analytical needs of fusion materials have been strong driving forces for simulation program developments: SDTrimSP was developed for calculating erosion yields and reflection coefficients for plasma-surface interaction research in fusion devices. The SIMNRA code was initially developed to cover the analytical needs of IBA in fusion devices; the development of surface roughness algorithms [125] was triggered by the rough surfaces found on samples from JET. ERDA measurements of helium in tungsten fuzz [126,127] were the starting point for the development of the STRUCTNRA code [123].

The computer simulation of ion beam analysis methods is highly developed and able to provide quantitative results even for highly complex samples, while inter-comparisons of various codes (often organized by the IAEA) demonstrated the principal correctness of these codes.

6. Challenges for quantitative IBA analysis of fusion materials

This chapter discusses a number of issues for IBA of fusion materials. Many of these issues are general problems of IBA, but some of them are more severe in the fusion context due to particular materials such as Be and D investigated in fusion research and the high degree of international cooperation.

The following recommendations arise from goals of enabling analysis of all relevant isotopes and elements present in current nuclear fusion concepts and finding all inter-laboratory results of the same samples within their respective error bars. Comparisons and joint experiments were carried out in the past, but so far a solid value for the international repeatability of IBA results is not available. Deviations in the results could lead to false conclusions of expensive experimental campaigns. Missing analysis capabilities increase cost and reduce result quality.

6.1 Complex samples

RBS spectra from rough Mo/W layers on top of W are shown in Fig. 9. Such layer structures have been used for erosion/deposition studies in JET [128,129]. Both examples are challenging due to the large analysed thickness of more than 15 μm of high-Z elements, resulting in visible multiple-

and plural scattering effects (dotted lines), and due to the roughness of the substrate and the layers. The spectrum on the left sample can be simulated accurately (solid line), except channel numbers below about 200 where minor deviations between the experimental data and the simulation are observed. The simulation of the spectrum from the right sample requires an additional Lorentzian substrate roughness of 50° FWHM. The simulation still reproduces the main features of this spectrum, allowing extracting the mean thicknesses of the Mo and W layers. However, some details of the experimental spectrum are not well reproduced, so that this very complex rough sample marks the current limits of the simulation of inhomogeneous, rough samples. A simple simulation assuming smooth layers and without plural scattering (dashed lines) poorly reproduces the experimental spectra.

The influence of various types of surface roughness on the determination of depth profiles and total amounts of elements was investigated in [123] by computer simulations. It was concluded that roughness and depth profiles are generally ambiguous, but “total amounts of elements can be derived with some robustness from count integrals. For moderate roughness, not too large energy losses and sufficiently smooth cross-sections count integrals allow to determine total amounts of elements with an uncertainty of the order of less than 10%.”

The analysis of solidified melt zones, as shown in Fig. 3(d), is generally possible, but not straightforward and no user-ready recipes exist. This relates to the fact that melt damage may change the chemical composition, surface roughness and structure including the formation of cracks under heat loads. The effect of continued plasma exposure on intentionally melt-damaged divertor tiles was studied recently in ASDEX Upgrade and resulted in a microscopically very inhomogeneous erosion/deposition pattern on the corrugated pre-damaged surface. Net erosion was observed at surface areas oriented towards the incident plasma flux and net deposition in shadowed areas [131]. Moreover, the surface composition may be further modified by the exposure history after the damage had occurred. Therefore, individual approaches must be applied in studies of melt zones.

6.2 Input data for IBA

IBA measurements are indirect measurements, primarily yielding reaction probability spectra. The determination of the underlying sample composition and structure relies on the interpretation of these spectra via physical models as discussed in section 5 requiring additional input data. The accuracy of these input data therefore limits the accuracy of the IBA results, requiring precise input data on:

- Stopping powers;
- Energy straggling;

- Cross-section data for non-Rutherford scattering and nuclear reactions.

For the stopping power a solid physical understanding exists for energies above a few 100 keV/amu with the Bethe-Bloch equation. Additional corrections and fits to experimental data, in particular with the SRIM code [102,132], provide an accuracy of 4.0% for protons and deuterons, 3.9% for He isotopes, 4.8% for Li, and 5.8% for other ions in single-elemental targets [132]. These values are averaged over all elemental targets. However, the uncertainties are usually higher at energies in the region of the stopping power maximum and below and can exceed the overall inaccuracies given above. For a number of elements (e.g. transition metals) experimental stopping-power data can be very scarce or non-existent [133], resulting in larger (but hardly quantifiable) inaccuracies. Also for elements with interest to fusion the experimental data base is sometimes very poor: For He in Mo or W there are only 2 experimental data sets, respectively, in the region of the stopping power maximum. These deviate by 10-20% with the SRIM data lying in between [134].

Moreover, deposited layers in fusion devices typically contain a mixture of all elements present in the device: This material has sometimes been called tokamakium [135]. As experimental data on stopping powers in these mixed materials are extremely scarce or even non-existing, the stopping powers of these compounds have to be determined assuming a linear combination of the stopping contributions of all elements called ‘Bragg’s rule’ [136]. **This is normally done automatically by the analysis software but can get problematic if the layers contain large concentrations of carbon together with hydrogen isotopes, because deviations from Bragg’s rule of 10-20% have been observed in hydrocarbon materials including amorphous hydrocarbon layers [137]. Similar deviations from Bragg’s rule have also been observed in carbides, nitrides and oxides [138]. Simulation software often allow taking deviations from Bragg’s rule into account using an ad-hoc correction factor.** This problem is somewhat relaxed in today’s fusion devices with metallic walls, because deviations from Bragg’s rule are assumed to be small (typically < 2%) in metallic compounds and alloys [139], **and also in compounds containing heavier atoms such as Fe₂O₃, NbC, NbN, Ta₂O₅, WO₃ [138].**

Inaccuracies of stopping powers have a direct influence on the accuracies of derived elemental concentration profiles. For large samples an accurate measurement of the incident ion beam current is generally difficult, and the integrated charge is then often determined from a fit to the bulk spectrum. In this case, inaccuracies of the bulk stopping powers may have direct consequences also for the determination of total amounts of elements.

The slowing down of ions is always associated with energy straggling. Precise energy straggling data are required

for a correct description of the low-energy edge of smooth layers, for modelling the correct shape of spectra with narrow peaks in the cross-section, and for depth resolution calculations. Electronic energy loss straggling can be calculated using Bohr’s theory [140] with corrections for electron binding [141] and charge-state fluctuations [142] in order to achieve sufficient accuracy. For high-Z elements the energy spread introduced by multiple small-angle scattering can get important, an analytical theory of multiple scattering is presented in [108] and was shown to be in good agreement with MD and MC [143]. Geometrical energy spread introduced by finite beam spot size and detector aperture width can be treated analytically [108]. Overall, despite the general wish for more accurate data, the accuracy of straggling data is considered sufficient for the purposes of fusion investigations, where often surface or layer roughness dominate energy spread.

For the reaction cross-sections a fundamental physical model does not exist, hence these data have to be determined experimentally. Semi-empirical fitting models using R-matrix theory are available; here in particular the SigmaCalc [144] code is established in the IBA community, allowing for cross-section data interpolation if a sufficient amount of the 2D space of E and θ has been determined experimentally for a specific reaction with sufficiently high accuracy. This situation is desired as it allows for improved data quality via the combination of data involved in the fitting process and allows for corrections of detector size and position specific to the individual setups.

Currently the database of cross-sections is particular fragmentary for fusion materials. One example for the case of Be is demonstrated in figure 10. The p_0 and p_1 peaks from the ${}^9\text{Be}({}^3\text{He}, p_x){}^{11}\text{B}$ reaction are reproduced accurately in the simulation, but the remaining 9 lower-energy peaks cannot be simulated due to missing cross-section data. The decay of ${}^8\text{Be}$ (produced in the ${}^9\text{Be}({}^3\text{He}, \alpha_x){}^8\text{Be}$ reaction) into 2 α ’s results in an additional background which cannot be simulated correctly. For the analysis of deuterium retention using the $\text{D}({}^3\text{He}, p){}^4\text{He}$ nuclear reaction the angular distribution of the reaction products is almost isotropic in the center-of-mass system at ${}^3\text{He}$ energies below about 1200 keV [145]. At higher energies good datasets exist only for $\theta=135^\circ$, 144.5° and 175° [146,147]. Due to the lack of easily available alternatives, these datasets are widely applied even for different reaction angles. This practice leads to unknown systematic errors of the results in quantity and depth distribution.

In conclusion, on the basis of the cross-section data contained in IBANDL the authors identified the need for determining the cross-sections for D, Li, Be, C, N, O analysis (including all stable isotopes) with ${}^3\text{He}$ for angles of 120° - 175° and energies up to 6 MeV and the cross-sections for Li and Be analysis with protons for angles of 120° - 175° and

energies up to 4.5 MeV. Furthermore, the determination of stopping powers for specific fusion materials such as W in particular at low energies and up to 5 MeV protons and helium ions and for heavy ions (used in ERD) is recommended.

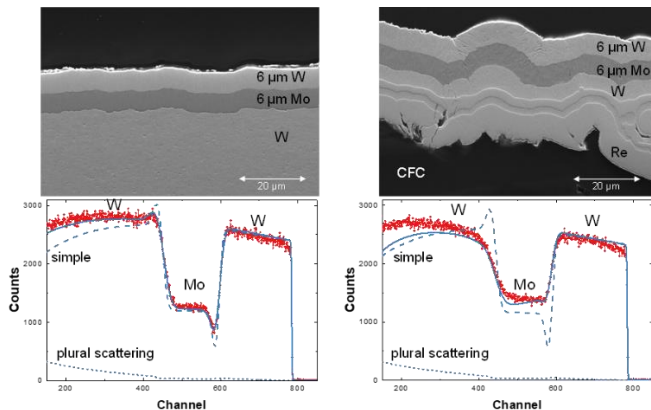


Figure 9. Top left: Cross-section of 6 μm Mo and W layers on bulk W. Top right: Cross-section of carbon-fibre composite (CFC) material, coated with a 14 μm Re and W layer, 6 μm Mo, and 6 μm W. Bottom: Experimental and simulated RBS spectra, measured with 4 MeV protons, backscattering angle 165° , normal incidence. Dashed line - simple simulation with smooth layers and without plural scattering; Dotted line - plural scattering contribution; Solid line - Simulation including substrate roughness (in the case of CFC), layer roughness, multiple and plural scattering. Simulations by SIMNRA [111,125]. Modified from [130].

^3He -based NRA is a major tool for the quantification and depth profiling of deuterium in PFCs [37-39,148] and in analyses of mixed materials containing deuterium, carbon (^{12}C , ^{13}C) and beryllium [149], as well as other low-Z species such as boron and nitrogen. Unfortunately, in studies carried out on beryllium substrates or Be-rich layers even a qualitative determination of the presence of carbon poses serious difficulties. While beryllium is of great importance as wall material for ITER and the metal is used in JET-ILW (see Chapter 2), the application of carbon is not foreseen in ITER [152] because of predicted unacceptable levels of tritium inventory [4,151,152]. However, carbon impurities are always present in vacuum systems and in many materials and eventually may have decisive impact on the retention. Therefore, a proper discrimination between beryllium and carbon is the prerequisite for accurate carbon quantification.

In figure 11 spectra of pure carbon and beryllium are shown for NRA with 3 MeV ^3He at 170° . In situations where the amount of C dominates over the Be content both elements can be easily distinguished because the Be concentration can be calculated from the high energy peaks. The C content is then calculated from the carbon peaks after subtraction of the beryllium background. In the reverse case the situation is much more complex as already small uncertainties in the beryllium cross-section will dominate over the carbon signal in the regions where peaks of both

elements coincide. Because the cross-section varies, it is especially difficult to ensure proper background subtractions for thicker samples where the cross-section and/or the concentration will vary dependent on the depth in the sample.

In some situations (i.e. small amounts of C distributed in a Be matrix) it will always be very difficult to perform this type of analysis but having a more reliable data set on Be cross-sections will increase also the sensitivity for carbon detection. For the $^{12}\text{C}(^3\text{He},p_x)^{14}\text{N}$ reaction IBANDL contains cross-section data at 165° for $^{12}\text{C}(^3\text{He},p_0)^{14}\text{N}$; data at 160° , 150° , 120° and 90° for $^{12}\text{C}(^3\text{He},p_{0,1,2})^{14}\text{N}$; and at 177° for $^{12}\text{C}(^3\text{He},p_{1,2})^{14}\text{N}$ in a relatively narrow energy range. The agreement of the different data sets is poor. For the reaction $^9\text{Be}(^3\text{He},p)^{11}\text{B}$, IBANDL comprises cross-section values only for three angles: 150° , 135° , 90° . In several analyses systems higher angles (such as 165° and 170°) are used. A larger selection of angles would provide more possibilities for the optimisation of measurements.

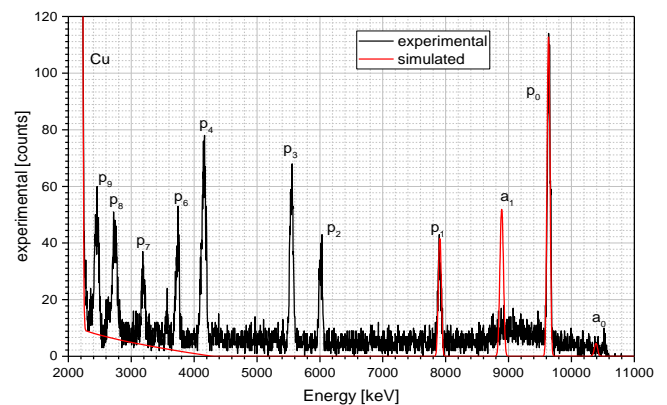


Figure 10. 2.95 MeV ^3He NRA/RBS analysis of a 1 μm thick Be film on Cu measured with a 1500 μm thick Si-Detector at 165° . SimNRA 7.01 analysis in red. Reaction products of $^9\text{Be}(^3\text{He},p_x)^{11}\text{B}$ and $^9\text{Be}(^3\text{He},\alpha_x)^8\text{Be}$ reactions are observed. From right to left α_0 , p_0 , α_1 , p_1 , p_2 , p_3 , p_4 , p_6 , p_7 , p_8 , p_9 , Cu RBS edge. Literature data on p_0 and p_1 well describe the measurement, but the other peaks are missing. ^8Be decay produced by the α -reactions induced an isotropic emission background.

Simultaneous quantification and depth profiling of Be and C can be performed by HIERDA, but the information depth is limited to several hundreds of nanometres. ERDA methods often require larger sample sizes and are difficult to use with μ -beams. Moreover, ERDA is very sensitive to the sample surface finishing due to the analysing beam grazing incidence requirement. Quantification of C in low-Z mixtures on beryllium has been achieved by means of deuterium-based NRA [153,154], but also in this case a comprehensive library of cross-sections would be beneficial.

Using higher incident energies increases the depth of analysis, but renders the availability of cross-section data even more difficult. Large depths of analysis can be achieved for example by combining IBA and SIMS or by cross-sectioning methods; TDS can deliver information about the

total amount of trapped hydrogen isotopes throughout the whole sample depth.

6.3 Standards

IBA work for fusion relies on sample analysis in numerous independent scientific institutions. Most of the applied devices are at least partially custom-made. Additionally, the quantitative evaluation of IBA measurements involves at larger number of manual adjustments (such as the selection of regions of interest) and the selection of input data (such as stopping powers or cross-section data). The ongoing developments of devices, analysis schemes/software, and input data, have led to a diverse situation where each laboratory (and sometimes even each researcher) uses different procedures for energy calibration, solid angle calibration, incident beam current measurement and data evaluation. This lack of standard procedures potentially leads to different results when analysing identical samples in different institutions. Potentially even the evaluation of the same raw IBA spectrum will lead to different results when performed by different scientists.

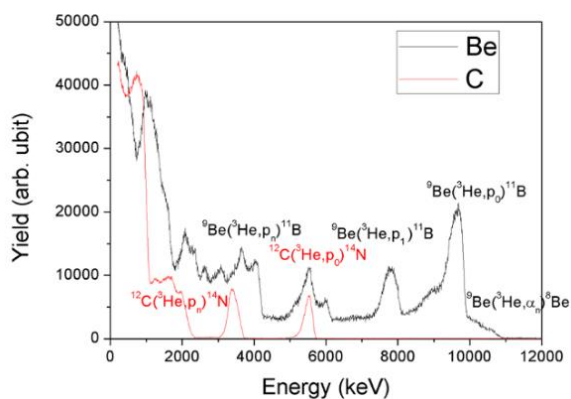


Figure 11. Spectra recorded with 3 MeV $^3\text{He}^+$ for pure carbon $^{12}\text{C}(^3\text{He},\text{p})^{14}\text{N}$ and beryllium $^9\text{Be}(^3\text{He},\text{p})^{11}\text{B}$, scattering angle 170° .

The analysis of data taken by means of IBA techniques involves several steps. Figure 12 demonstrates difficulties in selecting appropriate cross-sections in a situation where data exist. The four datasets disagree up to a factor 50 at practically identical reaction angles. Even if the analysis of C is not based on this elastic scattering, the contributions have to be taken into account as background for other reactions and for pile-up calculations.

In SIMNRA, NDF or other evaluation suites about 20 different calculation options exist for data analysis with potential strong influence on computing time and final results. In particular the applied stopping powers can introduce significant differences. The indirect nature of IBA measurements leads to the requirement of fitting procedures. This fitting can be executed manually or automatically, with different existing automatic algorithms (Simplex, Nead-Melder). A manual fitting cannot reach the accuracy of an

algorithm, but algorithms often have difficulties in fit convergence with the complex IBA spectra. The authors recommend evaluations and recommendations for the selection of input data and data evaluation procedures.

A definition of standards for data acquisition, analysis, and uncertainties for IBA along these lines opens the perspective for a high degree of similarity of results produced by different labs, boosting the credibility and scientific impact of IBA. For the scientific proof of this success, the authors recommend a round-robin test with samples specific for fusion. The selection of samples should be drawn along the line of expected systematic differences between the labs and probe the potentially weakest points. The technically probable differences are considered to lie in angular accuracy of detectors and samples due to alignment and tolerances, beam energy, and the integration of beam charge/secondary electron correction (Particle*Sr). These differences transfer to differences in measured total elemental content, layer thicknesses, and stoichiometry. The authors therefore suggest a round robin test for the determination of D retention in W and bulk and composition analysis of μm thin films.

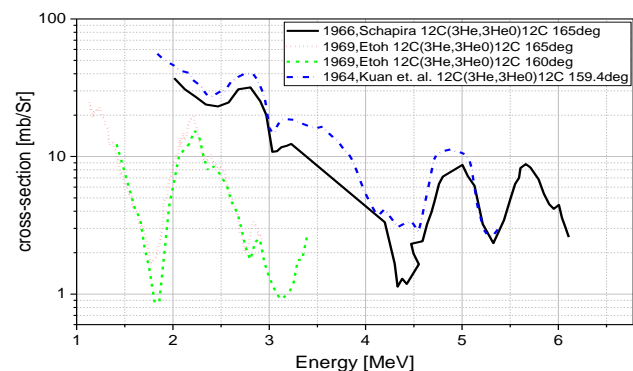


Figure 12. The cross-sections for non-Rutherford elastic scattering of ^3He from ^{12}C available in IBANDL exhibit differences over orders of magnitude in spite of similar conditions.

7. Conclusions

We have demonstrated the importance of ion-beam analysis for fusion research, connected to the presence of special elements such as Be and isotopes such as D, T, ^{15}N , and other tracers, and the importance of full compositional analysis including minute quantities for understanding the underlying plasma-surface interactions. In addition, we discussed the challenging requirements for ion-beam analysis in fusion research arising from the broad range of isotopes and elements, required input data, layered sample structures, sample roughness, sample size and mapping, and the handling of hazardous materials.

The high level of international cooperation in fusion research yields advantages by providing a high variety of exposure and analysis setups optimized for different tasks inside the fusion project, but also results in problems of inter-

comparability and standardisation. The success of the IBA community and its advantage for fusion research strongly rely on the credibility and acceptance of the technique.

Therefore, the authors conclude the following recommendations for future activities with details given in the preceding chapters:

- Provision of facilities for handling of hazardous materials (tritium, activated samples, beryllium) for existing experiments and ITER;
- Standardisation of measurement and evaluation procedures;
- Determination and possibly evaluation of cross-sections and stopping powers for elements and isotopes with relevance for fusion;
- International round-robin test with fusion relevant samples for determining the accuracy and comparability of different laboratories.

References

- [1] Federici G *et al*, 2001 *Nucl. Fusion* **41** 1967
- [2] Hofer W O and Roth J (Eds), *Physical Processes of the Interaction of Fusion Plasmas with Solids*, Academic Press, New York, 1996.
- [3] Philipps V *et al*, 2002 *Vacuum* **70** 399
- [4] Roth J *et al*, 2009 *J. Nucl. Mater.* **390-391** 1
- [5] Rubel M *et al*, 2013 *J. Nucl. Mater.* **438** S1204
- [6] Ström P *et al*, 2016 *Rev. Sci. Instrum.* **87** 103303
- [7] Kantre K *et al*, *Nucl. Instrum. Methods Phys. Res. B*, submitted
- [8] Bykov I *et al*, 2016 *Nucl. Instrum. Methods Phys. Res. B* **371** 370
- [9] Linnarsson M K *et al*, 2012 *Rev. Sci. Instrum.* **83** 095107
- [10] Ström P *et al*, 2017 *Nucl. Mater. Energy* **12** 472
- [11] Draxler M *et al*, 2004 *Vacuum* **73** 39
- [12] Markin S N, PhD thesis, JKU Linz (2008)
- [13] Foteinou V *et al*, 2018 *Phys. Rev. C* **97** 035806
- [14] Apostolopoulos G *et al*, 2016 *Nucl. Mater. Energy* **9** 465
- [15] Vlastou R *et al*, 2007 *J. Radional. Nucl. Chem.* **272** 219
- [16] Widdowson A *et al*, 2014 *Phys. Scr.* **T159** 014010
- [17] Baron-Wiechec A *et al*, 2015 *J. Nucl. Mater.* **463** 157
- [18] Widdowson A *et al*, 2017 *Nucl. Mater. Energy* **12** 499
- [19] Widdowson A *et al*, 2017 *Nucl. Fusion* **57** 086045
- [20] Catarino N *et al*, 2017 *Phys. Scr.* **T170** 014059
- [21] Raepsaet C *et al*, 2009 *Nucl. Instrum. Methods Phys. Res. B* **267** 2245
- [22] Bernard E *et al*, 2013 *J. Nucl. Mater.* **43**, S975
- [23] Uglov V V *et al*, 2015 *Nucl. Instrum. Methods Phys. Res. B* **354** 264
- [24] Linsmeier Ch *et al*, 2001 *Phys. Scr.* **T94** 28
- [25] Möller S *et al*, 2018 *Nucl. Mater. Energy* **17** 9
- [26] Martynova Y *et al*, 2017 *Nucl. Mater. Energy* **12** 648
- [27] Windmüller A *et al*, 2018 *Solid State Ionics* **320** 378
- [28] Behrisch R *et al*, 2000 *J. Nucl. Mater.* **281** 42
- [29] Peeper K *et al*, 2013 *J. Nucl. Mater.* **438** S887
- [30] Peeper K *et al*, 2014 *Phys. Scr.* **T159** 014070
- [31] Lessmann M T *et al*, 2017 *J. Nucl. Mater.* **486** 34
- [32] Fazinić S *et al*, 2018 *Anal. Chem.* **90** 5744
- [33] Hakola A *et al*, 2017 *Nucl. Fusion* **57** 066015
- [34] Brezinsek S *et al*, 2017 *Nucl. Fusion* **57** 116041-1
- [35] Pucella G *et al*, 2017 *Nucl. Fusion* **57** 102004-1
- [36] Caniello R *et al*, 2017 *Nucl. Mater. Energy* **10** 9
- [37] Wielunska B *et al*, 2016 *Nucl. Instrum. Methods Phys. Res. B* **387** 103
- [38] Wielunska B *et al*, 2019 *Nucl. Instrum. Methods Phys. Res. B* **440** 202
- [39] Mayer M *et al*, 2009 *Nucl. Instrum. Methods Phys. Res. B* **267** 506
- [40] Langley R A *et al*, 1974 *J. Nucl. Mater.* **53** 257
- [41] Schwarz-Selinger T, 2017 *Nucl. Mater. Energy* **12** 683
- [42] Mayer M *et al*, 2018 *Nucl. Mater. Energy* **17** 146
- [43] Farrokhi S *et al*, Bulletin d'Information Scientifique et Technique du CEA, No. 72 (1972) 65
- [44] Kakuee O *et al*, 2012 *Acta Phys. Polonica A* **122** 132
- [45] Jokar A *et al*, 2018 *Nucl. Instrum. Methods Phys. Res. B* **431** 25
- [46] Kakuee O *et al*, 2016 *Nucl. Instrum. Methods Phys. Res. B* **371** 156
- [47] Mokhles F. *et al*, 2016 *Nucl. Instrum. Methods Phys. Res. B* **373** 80
- [48] Nikbakht T *et al*, 2018 *Ultramicroscopy* **186** 112
- [49] Vavpetič P *et al*, 2017 *Nucl. Instrum. Methods Phys. Res. B* **404** 69
- [50] Kelemen M *et al*, 2017 *Phys. Scr.* **T170** 014067
- [51] Kelemen M *et al*, 2017 *Nucl. Instrum. Methods Phys. Res. B* **404** 179
- [52] Markelj S *et al*, 2016 *J. Nucl. Mater.* **469** 133
- [53] Markelj S *et al*, 2017 *Nucl. Mater. Energy* **12** 169
- [54] Založnik A *et al*, 2016 *Nucl. Instrum. Methods Phys. Res. B* **371** 167
- [55] Vogel-Mikuš K *et al*, 2009 *Nucl. Instrum. Methods Phys. Res. B* **267** 2884
- [56] Martin J A *et al*, 1988 *Appl. Phys. Lett.* **52** 2177
- [57] Yu N *et al*, 1995 *Nucl. Instrum. Methods Phys. Res. B* **99** 566
- [58] Barton J L *et al*, 2014 *Nucl. Instrum. Methods Phys. Res. B* **332** 275
- [59] Simmonds M J *et al*, 2017 *J. Nucl. Mater.* **494** 67
- [60] Pathak S *et al*, 2017 *Scientific Reports* **7** 11918
- [61] Cui S *et al*, 2018 *J. Nucl. Mater.* **511** 141
- [62] Chen D *et al*, 2017 *Science Advances* **3** eaao2710
- [63] Qin W J *et al*, 2018 *Acta Materialia*, **153** 147
- [64] Ahlgren T *et al*, 2006 *Nucl. Instrum. Methods Phys. Res. B* **249** 436
- [65] Palonen V *et al*, 2016 *Nucl. Instrum. Methods Phys. Res. B* **380** 11
- [66] Väyrynen K *et al*, 2019 *Chemistry of Materials* **31** 5314
- [67] Ahlgren T *et al*, 2019 *Nucl. Fusion* **59** 026016
- [68] Heikinheimo J *et al*, 2019 *APL Mater.* **7** 021103
- [69] www.sandia.gov/research/facilities/technology_deployment_centers/ion_beam_lab/accelerators.html
- [70] www.psf.mit.edu/research/topics/accelerators-detectors
- [71] Hartwig Z S and Whyte D G, 2010 *Rev. Sci. Instrum.* **81** 10E106
- [72] Hartwig Z S *et al*, 2013 *Rev. Sci. Instrum.* **84** 23504
- [73] Sun C *et al*, 1989 *Nucl. Instrum. Methods Phys. Res. B* **40/41** 714
- [74] Hinks J A *et al*, 2011 *Vac. Sci. Technol. A* **29** 021003
- [75] El-Atwani O *et al*, 2018 *Acta Materialia* (in press)

- [76] Kirk M A *et al*, 2018 *J. Nucl. Mater.* **498** 199
- [77] Li Meimei *et al*, 2012 *Phil Mag.* **92** 2048.
- [78] Tsitroni E *et al*, 2009 *Nucl. Fusion* **49** 075011
- [79] Weckmann A *et al*, 2018 *Nucl. Mater. Energy* **17** 83
- [80] Rubel M *et al*, 2017 *Matter. Rad. Extrem.* **2** 87
- [81] Rubel M *et al*, 2016 *Nucl. Instrum. Methods Phys. Res. B* **371** 4
- [82] Coad J P *et al*, 2018 *Fusion Eng. Des.* **138** 78
- [83] Rubel M *et al*, 2017 *Nucl. Fusion* **57** 066027
- [84] Rubel M *et al*, 2013 *J. Nucl. Mater.* **438** S1204
- [85] Krat S. *et al*, 2017 *Nucl. Mater. Energy* **12** 548
- [86] Widdowson A *et al*, 2017 *Phys. Scr.* **T170** 014060
- [87] Widdowson A *et al*, 2016 *Phys. Scr.* **T167** 014057
- [88] Rubel M *et al*, 1989 *J. Nucl. Mater.* **161** 153
- [89] Scherzer B M U private communication
- [90] Markelj S *et al*, 2019 *Nucl. Fusion* **59** 086050
- [91] Rubel M *et al.*, 2007 *J. Nucl. Mater.* **365-367** 877
- [92] Wang W *et al*, 1997 *J. Nucl. Mater.* **245** 66
- [93] Wielunska B *et al*, to be published
- [94] Mayer M *et al*, 2001 *J. Nucl. Mater.* **290-293** 381
- [95] Frenkel D. and Smit, 2002 Understanding Molecular Simulation: From Algorithms to Applications, *Computational Science Series Vol. 1*, ISBN-13:978-0122673511, Academic Press
- [96] Nordlund K *et al*, 2018 *Nature Communications* **9** 1048
- [97] Nordlund K 1995 *Computational Materials Science* **3** 448
- [98] Nordlund K *et al*, 2016 *Phys. Rev. B* **94** 214109
- [99] Robinson M and Torrens I, 1974 *Phys. Rev. B* **9** 5008
- [100] Biersack J P *et al*, 1991 *Nucl. Instrum. Methods Phys. Res. B* **61** 77
- [101] Eckstein W and Mayer M, 1999 *Nucl. Instrum. Methods Phys. Res. B* **153** 337
- [102] Ziegler J F, Biersack J P and Ziegler M D, 2008 SRIM - The Stopping and Range of Ions in Matter, ISBN 978-0-9654207-1-6 SRIM Co., Chester
- [103] Mutzke A, Schneider R, and Dohmen R, 2011 SDTrimSP: Version 5.00. IPP, Report, (12/8), <http://hdl.handle.net/11858/00-001M-0000-0026-EAF9-A>
- [104] Hofsäss H *et al*, 2014 *Appl. Surf. Sci.* **310** 134
- [105] Arstila K *et al.*, 2001 *Nucl. Instrum. Methods Phys. Res. B* **174** 163
- [106] Arstila K *et al*, 2004 *Nucl. Instrum. Methods Phys. Res. B* **219-220** 1058
- [107] Schiettekatte F. 2008 *Nucl. Instrum. Methods Phys. Res. B* **266** 1880
- [108] Szilagyí E *et al*, 1995 *Nucl. Instrum. Methods Phys. Res. B* **100** 103
- [109] Rauhala E *et al*, 2006 *Nucl. Instrum. Methods Phys. Res. B* **244** 436
- [110] Mayer M, SIMNRA Users Guide, Report IPP 9/113, Max-Planck-Institut für Plasmaphysik, Garching, Germany, 1997. <http://hdl.handle.net/11858/00-001M-0000-0027-6157-F>
- [111] Mayer M, 2014 *Nucl. Instrum. Methods Phys. Res. B* **332** 176
- [112] Barradas N P *et al*, 1997 *Applied Physics Letters* **71** 291
- [113] Doolittle L R, 1985 *Nucl. Instrum. Methods Phys. Res. B* **9** 344
- [114] Barradas N P *et al*, 2007 *Nucl. Instrum. Methods Phys. Res. B* **262** 281
- [115] Barradas N P *et al*, 2008 *Nucl. Instrum. Methods Phys. Res. B* **266** 1338
- [116] Silva T F *et al*, 2016 *Nucl. Instrum. Methods Phys. Res. B* **371** 86
- [117] Schmid K and von Toussaint U, 2012 *Nucl. Instrum. Methods Phys. Res. B* **281** 64
- [118] Mutzke A. *et al*, 2011 *Nucl. Instrum. Methods Phys. Res. B* 269 582
- [119] Mayer M and Lederer S, 2019 *Nucl. Instrum. Methods Phys. Res. B* **453** 67
- [120] Mayer M. and Silva T F, 2017 *Nucl. Instrum. Methods Phys. Res. B* **406** 75
- [121] Mutzke A, Schneider R, Bandelow G, SDTrimSP-2D: Simulation of Particles Bombarding on a Two Dimensional Target-Version 2.0, Report IPP 12/11, Max-Planck-Institut für Plasmaphysik, Garching, Germany, 2013. <http://hdl.handle.net/11858/00-001M-0000-0026-E06F-E>
- [122] Schiettekatte F and Chicoine M, 2016 *Nucl. Instrum. Methods Phys. Res. B* **371** 106
- [123] Mayer M, 2016 *Nucl. Instrum. Methods Phys. Res. B* **371** 90
- [124] Mayer M *et al*, 2016 *Nucl. Instrum. Methods Phys. Res. B* **385** 65
- [125] Mayer M, 2002 *Nucl. Instrum. Methods Phys. Res. B* **194** 177
- [126] Woller K B *et al*, 2013 *J. Nucl. Mater.* **438** S913
- [127] Woller K B *et al*, 2015 *J. Nucl. Mater.* **463** 289
- [128] Mayer M *et al*, 2016 *Phys. Scr.* **T167** 014051
- [129] Mayer M *et al*, 2017 *Phys. Scr.* **T170** 014058
- [130] Mayer M *et al*, 2011 *Nucl. Instrum. Methods Phys. Res. B* **269** 3006
- [131] Krieger K *et al*, 2019 *Phys. Scr.* (in press)
- [132] www.srim.org
- [133] Wittmaack K, *Nucl. Instrum. Methods Phys. Res. B* **380** (2016) 57
- [134] <https://www.nds.iaea.org/stopping/>
- [135] Behrisch R *et al*, 1996 *J. Nucl. Mater.* **233-237** 673
- [136] Bragg W H and Kleeman R, 1905 *Philos. Mag.* **10** 318
- [137] Boutard D *et al*, 1988 *Phys. Rev. B* **38** 2988
- [138] Ziegler J F and Manoyan J M, 1988 *Nucl. Instrum. Methods Phys. Res. B* **35** 215
- [139] Feng J S-Y *et al*, 1973 *Thin Solid Films* **19** 227
- [140] Bohr N, 1948 *Matter, Mat. Fys. Medd. Dan. Vid. Selsk.* **18** 8
- [141] Chu W K, 1976 *Phys. Rev.* **13** 2057
- [142] Yang Q *et al*, 1991 *Nucl. Instrum. Methods Phys. Res. B* **61** 149
- [143] Mayer M *et al*, 2006 *Nucl. Instrum. Methods Phys. Res. B* **249** 823
- [144] Abriola D. *et al*, 2011 *Nucl. Instrum. Methods Phys. Res. B* **269** 2972
- [145] Nocente M *et al*, 2010 *Nucl. Fusion* **50** 055001
- [146] Alimov V Kh *et al*, 2005 *Nucl. Instrum. Methods Phys. Res. B* **234** 169
- [147] Wielunska B *et al*, 2005 *Nucl. Instrum. Methods Phys. Res. B* **371** 41
- [148] Rubel M. *et al*, 1997 *J. Nucl. Mater.* **241-243** 1026
- [149] Rubel M *et al*, 2005 *Vacuum* **78** 255
- [150] Merola M *et al*, 2014 *Fusion Eng. Des.* **89** 890
- [151] Coad J P *et al*, 2001 *J. Nucl. Mater.* **290-293** 224
- [152] Rubel M *et al*, 2003 *J. Nucl. Mater.* **313-316** 321
- [153] Lagoyannis A *et al*, 2017 *Nucl. Fusion* **57** 076027

- [154] Tsavalas P *et al*, 2017 *Phys. Scr.* **T170** 014049
- [155] Rubel M, 2006 *Phys. Scr.* **T123** 54
- [156] Balvanović R *et al*, 2012 *Nucl. Instrum. Methods Phys. Res.*
A **690** 17
- [157] Tesmer J R *et al*, 1987 *MRS Bulletin* **12** 101